The Effect of the Mixing Model on the Characteristics of Cu-Ni-Mo-4SiC Composite Synthesized by Powder Metallurgy

UDC:621.762:669.35
Original scientific paper https://doi.org/10.46793/aeletters.2026.11.3.1

Suprianto[1*], Agnes Maysa Salsabila[1], Fadly Ahmad Kurniawan Nasution[1], Ade Irwan[1], Irfan Sitorus[2], Bakhrul Ilmi[2]

[1]Department of Mechanical Engineering, Faculty of Engineering, Universitas Sumatera Utara, Jl. Almamater Kampus USU, Padang Bulan, Medan 20155, Indonesia
[2]Mechanical Engineering Graduate Study Program, Faculty of Engineering, Universitas Sumatera Utara, Jl. Almamater Kampus USU, Padang Bulan, Medan 20155, Indonesia

Abstract:
The mixing method plays a decisive role in achieving microstructural uniformity and in defining the mechanical, tribological, and electrical performance of composite materials. This study aims to evaluate the characteristics of a Cu-Ni-Mo-4SiC composite produced using various powder mixing models. The composites were prepared through powder metallurgy employing horizontal mixing (HM), V-mixer blending (VM), and mechanical alloying (MA). The powders were mixed further, compacted at room temperature, and subsequently sintered at elevated temperatures. The resulting composites were examined using various characterization methods, including Scanning Electron Microscope (SEM) - Energy Dispersive Spectroscopy (EDS) for microstructural observation, X-ray Diffraction (XRD) for crystal structure identification, measurements of density, Vickers microhardness, wear resistance, and electrical conductivity at room temperature. The results show that mechanical alloying led to a finer crystallite size, a more homogeneous Cu-Ni matrix, better distribution of Mo and SiC particles, and reduced porosity. Hence, the highest performance was attained in the MA composite, which has a hardness of 65.1 HV, specific wear rate of 5.56×10^{-5} mm^3/Nm, electrical conductivity of 62% IACS, and resistivity of 2.78×10^{-8} Ωm. This can be explained by finer grains, reduced particle aggregation, and even dispersion strengthening. As a result, under electrical service at room temperature and dry sliding load of 10 N for 20 min, the MA composite could serve as a material for electrodes and sliding electrical parts.

ARTICLE HISTORY
Received: 28 December 2025
Revised: 25 July 2026
Accepted: 7 August 2026
Published: 23 September 2026

KEYWORDS
Mechanical alloying, Hardness, Homogeneity, Microstructure, Specific wear rate

1. INTRODUCTION

Copper-matrix composites (CMCs) have found wide application in electrical contacts, welding electrodes, switches, circuit breakers, thermal management applications, and electrical sliding contacts due to their high electrical and thermal conductivity, along with mechanical and tribological properties [1]. Nanoparticles of Al_2O_3 and whiskers of SiC could enhance the mechanical properties of Cu composites via fine grain, dispersion hardening, load transfer, and the Orowan effect [2]. Reinforcement in the form of Ti_3SiC_2 has also been found to enhance the mechanical and wear resistance of Cu-Ni-Si powder metallurgy-based composites [3]. The above factors, however, could hinder densification due to agglomeration, poor interfacial bonding, and porosity [1].

The Cu-Ni alloy system was chosen as the metal matrix since copper and nickel have a face-centred

*CONTACT: Suprianto, e-mail: suprianto@usu.ac.id

cubic (FCC) structure and form a wide solid solution [4]. Mechanical attrition is known to cause solid solution hardening through increased defect density and decreased grain size [5]. In this particular composition, Cu serves as the main conductor, while Ni provides solid-solution strengthening and wear resistance [3, 4].

The mechanism of solid-state mixing using MA involves plastic deformation, cold welding, fracturing, and re-welding of the powder particles [6]. These lead to the creation of new interfaces, dislocations, vacancies, and grain boundaries, thereby reducing the diffusion distance and improving atomic mobility. The milling rate, time, and the ball/powder ratio determine particle size reduction, lattice strain, and eventual sintering behaviour [7]. For Mo-Cu systems, densification still largely depends on particle size, interfacial contact, and sintering due to the very limited solubility between them [8]. Mo has been added as a reinforcing phase for enhanced hardness, wear resistance, and mechanical strength. The production of a Cu-5 wt.% Mo alloy via powder metallurgy resulted in high hardness and conductivity, demonstrating Mo's ability to strengthen Cu while maintaining its electrical conductivity [9]. However, Mo particles could change the surface properties of Cu powders. Despite its high melting point and poor diffusivity, segregation of the Mo-rich phase is likely due to inadequate refinement and dispersion of Mo particles [10]. Addition of SiC was done to prevent plastic deformation and abrasion of the material in the sliding conditions. It has been reported that the addition of Ni increases corrosion resistance, while the addition of SiC increases hardness and wear resistance in contact electrodes [11]. The properties such as density, porosity, hardness, wear resistance, and electrical conductivity depend on the particle size and distribution of SiC [12]. Fine particles of SiC tend to agglomerate due to their higher surface area and different sizes, densities, and flow behaviour compared with metal powder [1].

The three mixing methods being considered have different mechanisms for creating powder flow and energy transfer. Tumbler mixers create circulation of particles due to rolling and cascading actions; however, their performance is powder-dependent and condition-dependent [13]. VMs create powder bed segregation by dividing it and mixing it several times, though particles with different sizes and inertia might have different movement and segregation patterns [14]. The conditions of powder mixing affect the dispersion of reinforcements, shrinkage, microstructure and properties of the product [15]. The quality of homogenization also affects the mechanical and tribological properties of powder metallurgy composites [16]. The milling time, milling speed, and impact energy affect the mechanical deformation, dispersion, and strength of particles [17]. Low-energy mixers can be effective for mixing bulk particles; however, they cannot separate strongly bonded reinforcement particles [18]. Thus, HM will provide the base level of bulk mixing, VM will improve it, and MA will achieve maximum homogenization and particle refinement.

Particle distribution of reinforcements plays an important role in determining the mechanism of wear of Cu-based composite materials, since the behaviour of such materials is controlled by the deformation of the matrix, disintegration of particles, and the removal of abrasives from the surface [19]. Mo can be responsible for the improvement of tribological properties of the material through the creation of low shear Mo oxide films, but the effect will depend on the continuous nature of the film [20]. Mixing of materials can influence electrical conductivity through particle connectivity [21]. Small-scale variations in the mixing process have shown an effect on electrical resistivity [22].

Latest trends in advanced CMCs show that there is a need to achieve a proper compromise among strength, wear properties, and electrical conductivity through proper control of composition and microstructure [23]. However, a direct comparative analysis within HM, VM, and MA processes using the same composition and consolidation of Cu-Ni-5Mo-4SiC has not been previously reported. The investigation aims to study the effects of these mixing processes on phase structure, grain size, elemental segregation, density, porosity, hardness, friction coefficient, specific wear rate, and electrical conductivity. Novelty in this research includes the study of the relationships among powder flow process, mixing energy, microstructure, and material performance.

2. MATERIALS AND METHODS

In this study, Cu and Ni metallic matrix powders of purity ≥ 99.9% were utilized in this study, while Mo (99.9%) and SiC (98%) powders were used as reinforcements. All powder particles are characterised by an initial size below 40 µm. The Cu powder has a dendritic structure, whereas Ni, Mo, and SiC powders are of irregular structure. To

prevent excessive powder contamination, the powder was loaded into a glove box filled with argon. Each composition consisted of a 91 wt.% Cu-Ni matrix, containing 81.9 wt.% Cu and 9.1 wt.% Ni, corresponding to a Cu/Ni weight ratio of 90/10, along with 5 wt.% Mo and 4 wt.% SiC. Three techniques were applied for the mixing of powder: HM at 300 rpm for 2 h, VM at 120 rpm for 2 h, and MA at 1000 rpm for 2 h. The powders were processed in stainless-steel vials using 8.0 mm hard-steel balls at a ball-to-powder weight ratio (BPR) of 10:1, as illustrated in Fig. 1. The mixed powders from various models were compacted by using a hydraulic press with a single-acting cylinder at 250 MPa for a 15-minute holding time to produce green compacts with a diameter of 25.4 mm and a height of 7.11 mm. The extended holding was done to facilitate particle rearrangement and pressure equilibrium in the heterogeneous Cu-Ni-5Mo-4SiC powder mixture. The green compact was sintered in a muffle furnace at 770 °C for 1 hour. A low sintering temperature and short holding time were used to hinder excessive metal oxide formation. The heating rate was maintained at 16 °C/min up to 400 °C and then reduced to 10 °C/min until the sintering temperature was reached. This temperature is approximately 0.77 times the melting temperature of copper. This temperature was chosen to promote solid diffusion and particle bonding while preventing melting, excessive dimensional distortion, and grain growth.

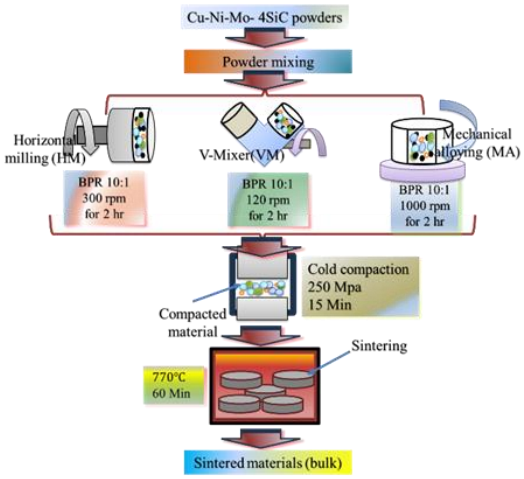

Fig. 1. Schematics of the synthesis of the Cu-Ni-Mo-4SiC using various mixing models: HM, VM, and MA

Furthermore, the properties of the sintered Cu-Ni-Mo-4SiC composite, starting with density, were determined using an analytical balance based on Archimedes' principle in accordance with ASTM B962. Vickers hardness was measured using a Shimadzu TMTECK HV1-100GB tester according to ASTM E92, with a 10 kgf load applied for 15 seconds. Dry friction wear test was conducted using a pin-on-disc tribometer according to ASTM G99 with a normal load of 10 N (0.127 MPa), friction speed of 6.28 m/s, friction distance of 7536 m, and time of 1200 s, where the pin has a diameter of 10 mm and a height of 10 mm against a disc of 170 mm diameter and a thickness of 9 mm made of AISI 52100 steel with a hardness of >800 HV. Electrical conductivity measurements were conducted using a Keithley 6517B Electrometer according to ASTM E1004, and the results are expressed in %IACS. In order to confirm the reliability and reproducibility of the experimental data, density, hardness, wear resistance, and electrical conductivity were measured on three different samples obtained by each mixing procedure, with their average values stated with standard deviations. Preparation of samples for SEM-EDS examination included sample polishing with the use of SiC grinding papers with grit sizes from 100 up to 2000. Polished surfaces were analysed without any chemical etching. Further microstructural and chemical composition studies of samples were carried out with the help of an Axia ChemiSEM LoVac scanning electron microscope with EDS, while phase characterization was performed using an X-ray diffractometer, Rigaku Mini Flex 600 type, with Cu-Kα radiation, model HyPix-400 MF 2D hybrid pixel array detector (HPAD) with Cu Kα radiation between 2-Theta = 20-80° at a scanning speed of 2 °/min. Moreover, the size of crystallites was estimated using the Scherrer equation, whereas the value of lattice strain was estimated using the Williamson-Hall approach.

3. RESULTS AND DISCUSSION

3.1. The XRD Spectra of the Cu-Ni-Mo-4SiC

The XRD patterns of various mixing models are demonstrated in Fig. 2. The Cu-Ni-Mo-4SiC predominantly FCC crystal structure consists of (111), (200), and (220) crystal planes dispersed at 43.3°, 50.4°, and 74.1° 2-Theta, which are associated with Cu and Ni-rich elements. A lower peak with the (110) at 40.6° 2-Theta is associated with a BCC structure and corresponds to the Mo element. Meanwhile, SiC peaks are not clearly visible due to their low volume fraction and overlap with the major Cu-Ni peaks; this particle is dispersed in the root peaks. Peak intensities vary with the mixing model used, as shown in Fig. 2.

The HM, which has low-impact energy during processing, resulted in the highest powder-stage

intensity. This fact might correlate with no significant change in the crystalline, plastic deformation, and crystallite size of the powder after the HM process. The VM shows relatively similar peak characteristics to the HM, with only a slight decrease in peak intensity. It is considered that the impact energy from grinding media causes deformation and reduces the crystallite size of the powder, further promoting a decrease in peak intensity. On the contrary, besides reducing peak intensity significantly, the MA causes peak broadening of the Cu-Ni-Mo-4SiC composite. Peak broadening is associated with strain, defects, and reduced grain size [24]. High energy from grinding media causes fracture, and cold welding occurs during the MA process, resulting in a finer particle size of the varying powders [25]. It is considered that the finer particles are correlated to the microstructural development and mechanical properties of various alloys.

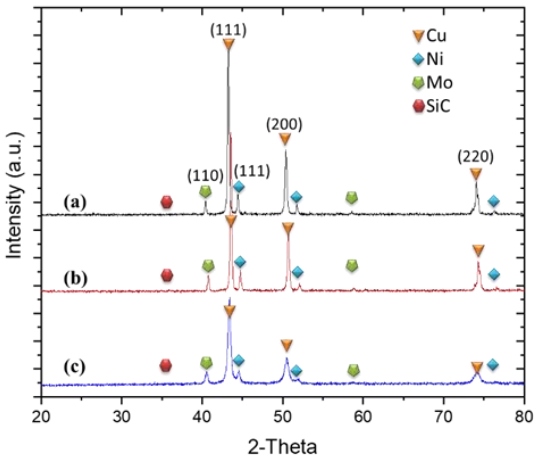

Fig. 2. X-ray diffraction spectra of Cu-Ni-Mo-4SiC powders for various mixing models: (a) HM, (b) VM, and (c) MA

Fig. 3 depicts the crystallite size and lattice strain of the powder stages of Cu-Ni-Mo-4SiC. The crystallite sizes decrease to 28 nm, 26 nm, and 12 nm for the HM, VM, and MA routes, respectively. The reduction of particle size through MA is attributed to the severe plastic deformation and repetitive fracturing-welding mechanism. A significant reduction in crystallite size of the powder was also obtained for Al-Cu-TiC material mixed by the MA technique [26].

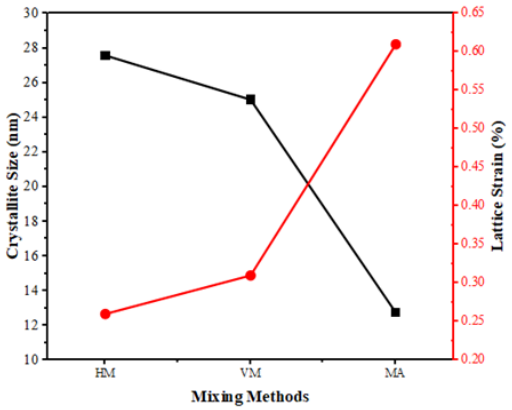

Fig. 3. The crystallite size of model Cu-Ni-Mo-4SiC composite with various mixing models: **(**a) HM, (b) VM, and (c) MA

The broadening of diffraction peaks in the XRD pattern demonstrates the formation of finer particles following MA. Furthermore, the lattice strain exhibits a notable increase with MA, as shown in Fig. 2. These results correspond to the mixing of CoCrCuFeMnNi powder mixed by MA [27]. Significant impact energy during MA introduces high stress and defects, promoting additional dislocations and micro-strain within the crystal lattice [28].

3.2. Microstructure of the Cu-Ni-Mo-4SiC

The microstructure of the sintered Cu-Ni-Mo-4SiC composite material via the HM process is presented in Fig. 4(a). It mainly contains the Cu-Ni-rich matrix along with some locally distributed Mo-rich particles less than 2 µm in size. These Mo-rich phases are observed to be brighter because of their high atomic numbers (Z = 42) compared to Cu (Z = 29) and Ni (Z = 28), leading to increased electron back-scatter and higher image contrast. This explanation can be correlated with the EDS results obtained from the SEM for point D, as shown in Fig. 4(b), and point F, as shown in Fig. 4(c), where the highest Mo concentration was found for the brightest regions of the surface. The presence of minor oxygen and carbon peaks is attributed to surface oxidation and carbon contamination during sintering. Furthermore, a finer microstructure with visible pores and more uniformly dispersed reinforcing particles was obtained for Cu-Ni-Mo-4SiC mixed by the V-mixer, see Fig. 4(b). The distribution of small SiC particles is visible within the solid solution phases, particularly in point C, which has high Si and C concentrations (see Table 1). The selected area at point D reveals that the composition is primarily made up of a Mo-rich

element with a concentration of more than 90 wt.% see Table 1. This Mo segregation was confirmed, as this element is hardly able to generate a solid solution in the Cu matrix. The segregation behaviour of this element was also investigated in the MoNi alloys [29]. The segregation of some refractory elements may be attributed to their high melting temperatures, which slow diffusion and promote elemental segregation. This phenomenon was also reported to occur for the V element in the CoCrCuFeNi alloy [30]. In line with the fact from Table 1, point D contains 90.7 wt.% Mo-rich with an element size of less than 2 µm, see Fig. 4(d). Furthermore, Fig. 4(c) demonstrates the microstructure of the Cu-Ni-Mo-4SiC mixed by the MA technique. Finer SiC and Mo particles were observed dispersed throughout the microstructure. It is considered that the high impact energy during MA promoted a finer particle size and crystallite size, as shown in Fig. 3. The selected area (point E) in Fig. 4(c) clearly consists of high Si and C peaks predominantly, as seen in Fig. 4(g). The SiC particles in Fig. 4(f) appear in an irregular form, with high-contrast regions adjacent to the Mo-rich point of F.

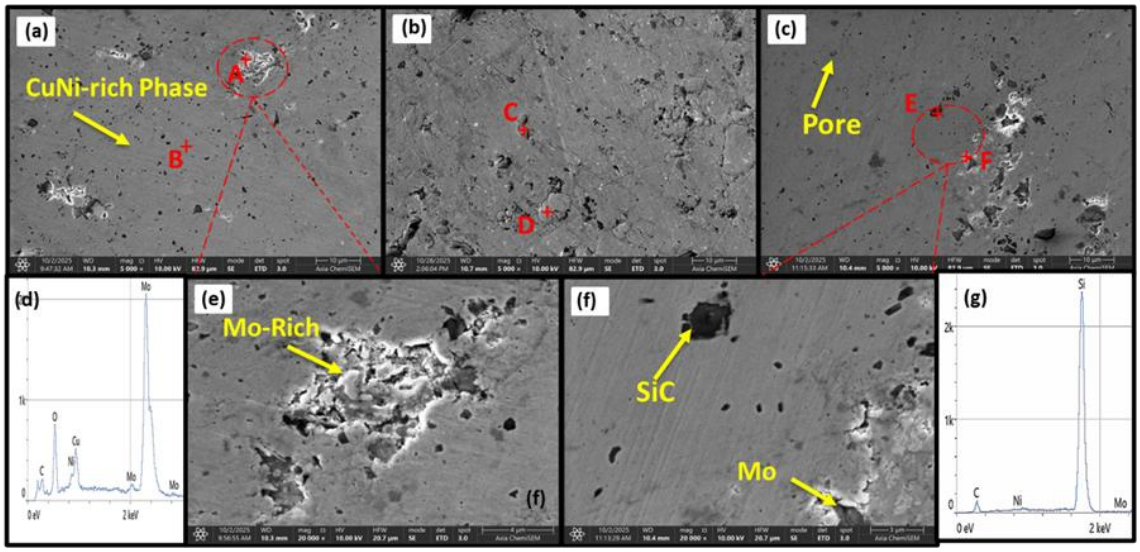

Fig. 4. SEM micrographs of sintered Cu-Ni-Mo-4SiC for various mixing models (a) HM, (b) VM, (c) MA, (e-f) enlarged area of SEM image, and (d, g) EDS spectra of selected areas

Table 1. Constituent elements of selected areas in Fig. 4

Mixing models	Points	Composition of the elements (wt.%)					
		Cu	Ni	Mo	Si	C	O
HV	A	10.3	1.8	75.1	0.2	1.8	10.8
	B	94.5	3.4	0.1	0.5	1.2	0.3
VM	C	22.7	5.4	0.6	36.2	2.3	32.8
	D	3.8	1.1	90.7	0.1	3.2	1.1
MA	E	1.0	0.0	0.0	87.3	11.4	0.3
	F	11.2	0.2	65.8	0.4	1.1	16.4

The Mo-rich observed in this Point F, in which 65.8 wt.% Mo is followed by the 16.4 wt.% O element dispersed at the segregation area, as shown in Fig. 4(e) and Table 1. In this microstructure, a small pore 1.5-3.0 µm in size was observed within the microstructure. The presence of micro-porosity tends to reduce the mechanical properties of the alloy; a similar phenomenon in the A2024 alloy was also reported [31]. The porosities may result from incomplete densification during compaction and sintering, which may affect mechanical and electrical properties. However, the presence of SiC and Mo in the Cu-Ni matrix contributes to improved strength. The involvement of Mo enhances the tensile strength and hardness of the Ti-Mo-Fe, which was also reported [32].

Fig. 5(a) shows the SEM analysis reveals the elemental distribution in the sintered Cu-Ni-Mo-4SiC composite obtained via horizontal milling. The grey area is identified as the FCC matrix, which consists of the Cu-Ni-rich elements. A homogeneous distribution of these elements was observed (see Figs. 5(b-c)). The clustered distribution of Mo was found using the Cu-Ni matrix;

see Fig. 5(d). This phenomenon corresponds to Fig. 4(d). The Mo element segregation could be attributed to its low diffusion rate during high-temperature sintering. The Mo segregation dispersed within the Ni-Mo matrix, especially along the grain boundary [33]. The Mo segregation dispersed in a similar location to O elements and was clustered within the microstructure, see Fig. 5(d-g). More O elements also dispersed near the porosity area were observed, as shown in Fig. 5(a-g). The existence of O in this area confirmed that the porosities were generated by gas entrapment during compaction [34]. Furthermore, the Si-rich elements were not distributed uniformly throughout the Cu-Ni matrix, as illustrated in Fig. 5(e). The EDS mapping also revealed the presence of the C element in small amounts dispersed throughout the microstructure. The presence of these particles (Si/C) tends to form some clustered areas and is dispersed in the microstructure as fragments within the microstructure of the Cu-Ni-Mo-4SiC composite, see Fig. 5(e). The fragment of a brittle SiC particle within the microstructure of the Cu-SiC synthesis by powder metallurgy was reported [35]. SiC and other ceramic particles are considered to have low wettability with the Cu matrix and to have the potential to form pores.

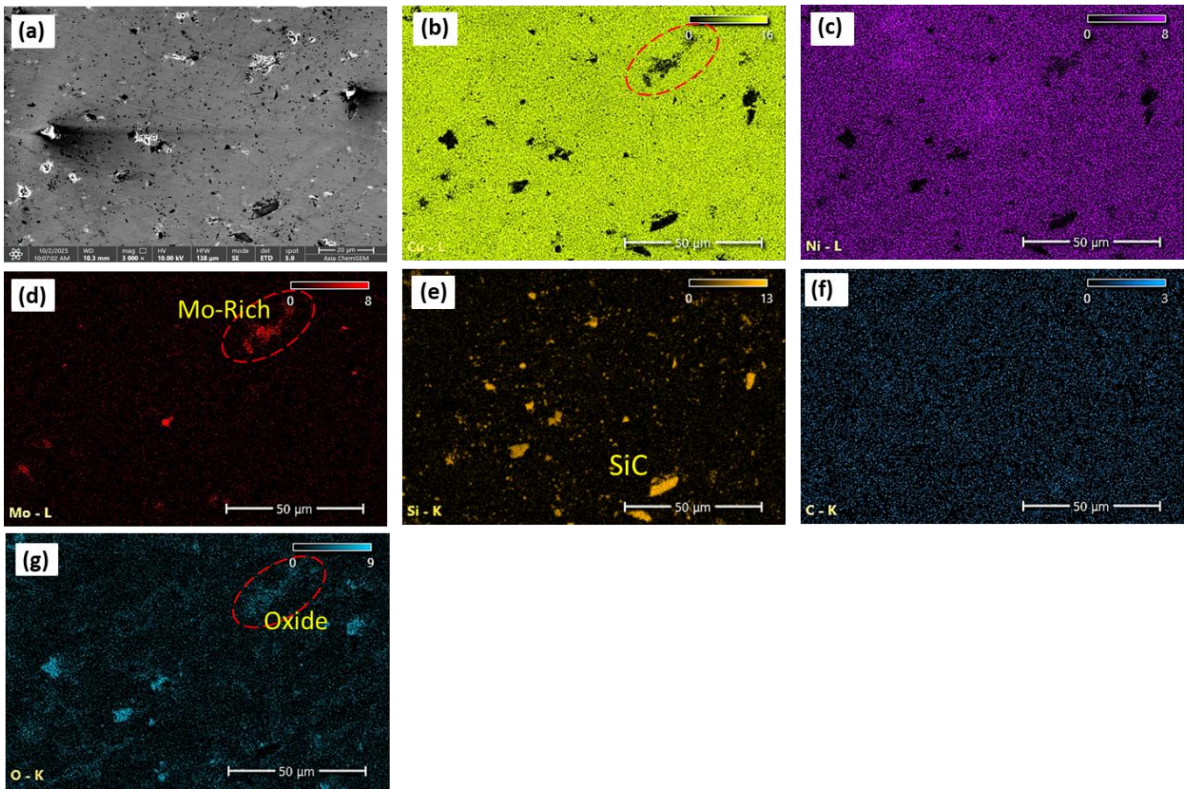

Fig. 5. (a) SEM images and (b) Cu maps, (c) Ni maps, (d) Mo maps, (e) Si maps, (f) C maps, and (g) O map for Cu-Ni-Mo-4SiC with HM

The SEM micrograph and elemental maps of the Cu-Ni-Mo-4SiC composite fabricated via MA are presented in Fig. 6(a). From Figs. 6(b-c), which present the Cu and Ni maps of the composite, it is clear that there exists a relatively uniform Cu-Ni matrix, while localized Mo-enriched regions are evident from Fig. 6(d). Discrete Si-enriched regions are evident in Fig. 6(e), which is the Si map of the composite and is linked to the SiC particles. The C map in Fig. 6(f) shows a broader distribution with some local enrichments. Finally, Fig. 6(g), which presents the O map of the composite, clearly indicates the presence of localized oxides in the composite.

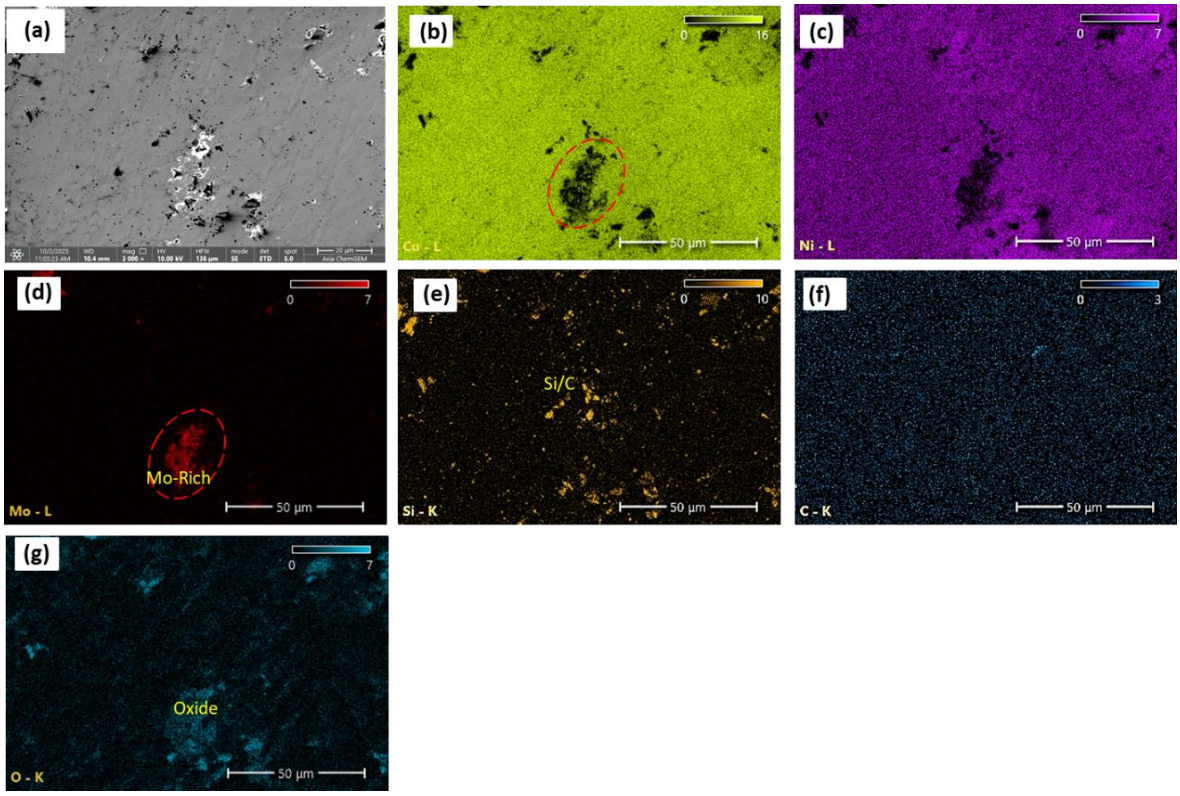

Fig. 6. (a) SEM images and (b) Cu maps, (c) Ni maps, (d) Mo maps, (e) Si maps, (f) C maps, (g) O map of the Cu-Ni-Mo-4SiC composite with MA

3.3. XRD Results for the Sintered Cu-Ni-Mo-4SiC Composite

Fig. 7 shows the XRD spectrum of Cu-Ni-Mo-4SiC composites with various mixing models. In the HM and VM mixing models, as seen in Fig. 7(a) and Fig.7(b), the diffraction peaks mainly consist of FCC solid solution phases with (111), (200), and (220) crystal planes, dispersed at angles of 43.0°, 50.1°, and 74.0° of 2-Theta, respectively. The presence of β-SiC is confirmed by the peak located at 35.6°, which indicates that SiC particles were retained without decomposition during the sintering process. The XRD results of the Cu-Ni-Mo-4SiC also showed the metal-oxide phase, which was detected at 35.6°, identified as Mo-oxide and Cu-oxide at 36°. These oxides formed during high-temperature sintering due to the higher affinity of the Mo element with O than other elements in this model alloy. This finding is consistent with the SEM-EDS results in Fig. 4, in which Cu and Mo are found in a similar location within the microstructure. The individual Mo element observed in the weak peak at 2-Theta 40.5° is considered to dissolve into the Cu-Ni matrix.

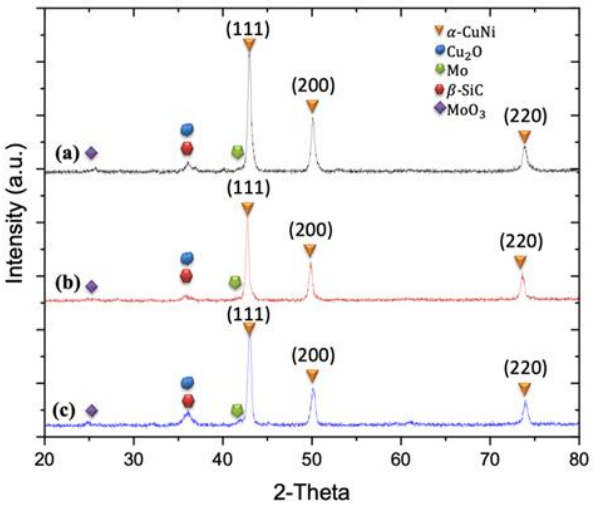

Fig. 7. XRD spectra of sintered Cu-Ni-Mo-4SiC composite for various mixing models (a) HM, (b) VM, and (c) MA

More broadening of Cu-Ni-Mo-4SiC was obtained for the MA mixing model, see Fig. 7(c). This broadening confirms that grain refinement and microstrain effects are induced by high-energy MA.

3.4. Hardness and Wear Properties

Fig. 8 illustrates the variation in hardness of the Cu-Ni-Mo-4SiC composites produced through various mixing models. The highest hardness, 65.1 HV, was obtained by using the MA mixing model. This method yields a finer crystallite size (see Fig. 3)

and a homogeneous distribution of SiC particles within the microstructure, as illustrated in Fig. 6. It is considered that these results contribute to the increased hardness of the Cu-Ni-Mo-4SiC composite. Meanwhile, the HM method produces the lowest hardness results, which are approximately 58.4 HV. Even though this method used a hard steel ball inside the cane, low impact energy resulted. This condition causes no significant reduction in particle size or crystallite size to be obtained, as shown in Fig. 3. The VM model demonstrates a slight increase in hardness (61.0 HV). This result could be linked to a slight decrease in the crystal size of the copper-based composite, which contributed to improving the hardness of Cu-Ni-MO-4SiC. In addition to the solid solution phase and particle strengthening, the presence of SiC particles has the potential to form pores near the Cu-Ni matrix and particles, see Fig. 4(a). The more porosity formed within the microstructure reduces the hardness of this Cu-Ni-Mo-4SiC. The increase in the porosity of the Cu-SiC-TiC with the addition of the SiC particles was reported [36].

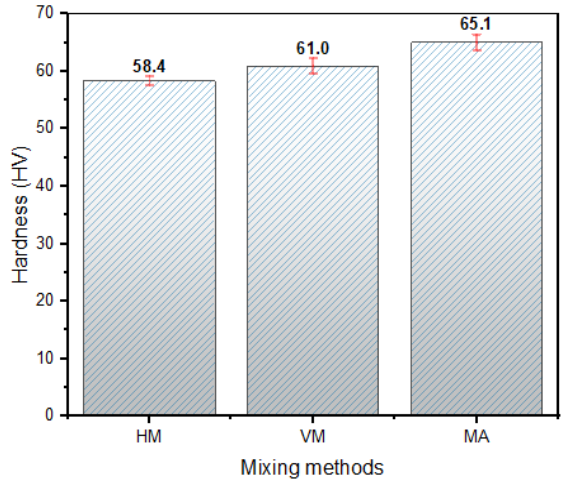

Fig. 8. Hardness of Cu-Ni-Mo-4SiC composite under various mixing models

Fig. 9 shows the specific wear rate of the Cu-Ni-Mo-4SiC using various mixing models. The highest specific wear rate of 18.5 x 10^{-5} mm^3/Nm occurred for the Cu-Ni-Mo-4SiC with the HM mixing model. The specific wear rate decreases to 14.8 × 10^{-5} mm^3/Nm and 5.56 x 10^{-5} mm^3/Nm when the VM and MA methods are used, respectively. These results align well with the hardness shown in Fig. 8, where the enhancement in hardness typically corresponds to a lower specific wear rate in the alloys. The reduction in the specific wear rate can be attributed to the formation of a homogeneous, fine-grained matrix with uniformly dispersed SiC particles, which effectively restricts plastic deformation and material removal during sliding. The role of the SiC in improving wear resistance during surface contact between Cu-SiC [37]. Significant wear resistance, attributed to the presence of Mo/SiC particles, was also reported in Cu-Mo-SiCs [38].

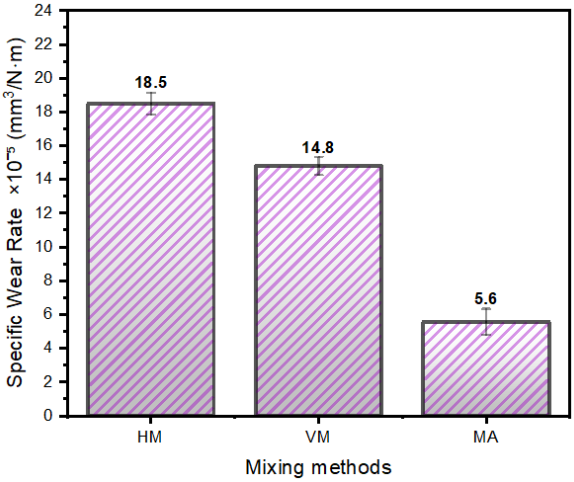

Fig. 9 illustrates the specific wear rate of Cu-Ni-Mo-4SiC for various mixing models, including (a) HM, (b) VM, and (c) MA approaches

The wear phenomenon is influenced by many factors, such as solid solution formation, reinforcement particles, pore defects, and wear conditions, whether dry or wet sliding. Fig. 10 demonstrates the friction coefficient during the wear test.

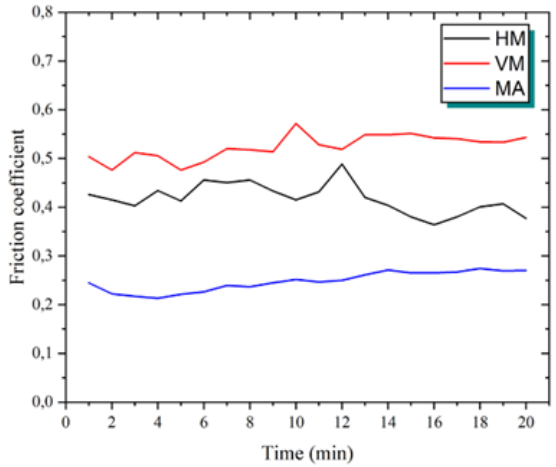

Fig. 10. The friction coefficient (μ) of the model Cu-Ni-Mo-4SiC composite with various mixing models

Fig. 10 clearly demonstrates the difference in the friction coefficient of the Cu-Ni-Mo-4SiC during sliding times from 0 to 20 min. The highest average friction was 0.5 and the lowest 0.2, obtained for the VM and the MA mixing models, respectively. The elevated coefficient value indicates that significant plastic deformation occurred across the surface of the Cu-Ni-Mo-4SiC composite, resulting in

increased particle detachment from the surface. This result is consistent with the highest specific wear rate recorded for the samples, as illustrated in Fig. 9. On the other hand, the HM and VM mixing models show that the μ values are not very different, with 0.4 of the friction coefficient in the HM mixing model.

As seen in Table 2, MA has the minimum Archard wear coefficient of 3.55×10^{-5}, which was around 66.5% less than HM and 59.9% less than VM. Therefore, it is evident that MA exhibited greater resistance to material removal under dry sliding conditions. The large reduction in specific wear rate k, even though there was only a small increase in hardness value, shows that it was not hardness alone that increased the wear resistance. Other reasons included a fine crystallite size, uniform dispersion of reinforcements, improved adherence between Mo and SiC particles, and reduced particle detachment.

Table 2. Hardness and wear parameters of Cu-Ni-5Mo-4SiC composites based on Archard's law.

Mixing Models	Hardness (HV)	Specific wear rate ($\times 10^{-5}$ mm³/Nm)	Archard wear coefficient (k)
HM	58.4	18.5	1.06×10^{-4}
VM	61.0	14.8	8.85×10^{-5}
MA	65.1	5.56	3.55×10^{-5}

Fig. 11 shows the surface morphologies and constituent elements of the selected area of wear prepared by various mixing models. The Cu-Ni-Mo-4SiC prepared by the HM method shows a rough surface with severe ploughing grooves, delamination, wear debris (see Fig.11(a)) and an oxide layer (see Fig.11(b)). This indicates that abrasive and adhesive wear are the predominant mechanisms.

Furthermore, Table 3 demonstrates the constituent elements of selected areas A and B on the surface contact. Point A in the wear matrix is predominantly made up of a Cu-Ni-rich particle. On the other hand, Point B had the highest Mo content as shown by the EDS spectrum of Fig. 11(c). This area consisted of 68.9 wt.% Mo, 18.2 wt.% O, and 8.0 wt.% Cu. The presence of high amounts of oxygen suggests high levels of oxidation through frictional wear, where the sliding process and frictional heating caused oxidation of the Mo and Cu-rich surfaces. The formation of oxides might temporarily prevent any metal-to-metal contact, but the fracturing and elimination of such a layer could lead to delamination and abrasive wear. The presence of O indicated surface oxidation and the probable development of some metal oxides on the surface of the Cu-Ni-Mo-4SiC composite during sliding contact.

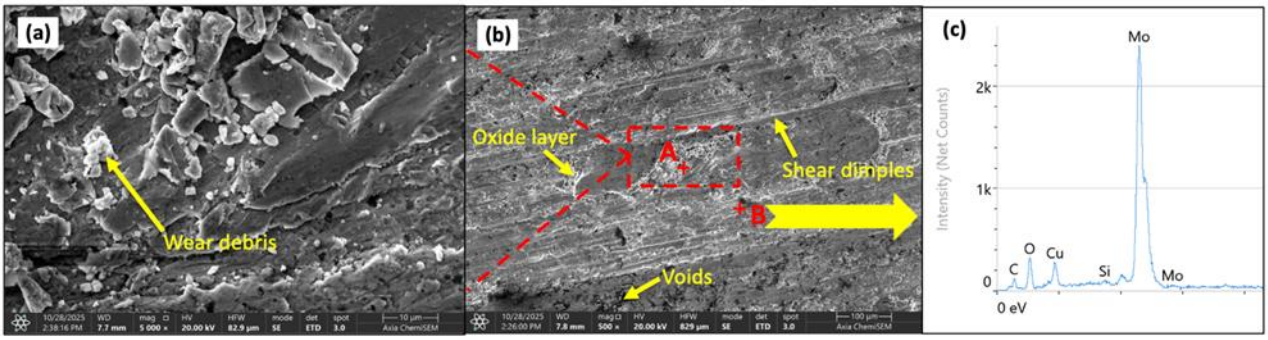

Fig. 11. (a) Enlarged area of the SEM image, (b) SEM image of the morphologies of the wear surface for HM, and (c) EDS spectra of selected areas of the Cu-Ni-Mo-4SiC composite (point B)

In contrast, the Cu-Ni-Mo-4SiC prepared by MA exhibits a much smoother wear track with fine debris particles and parallel grooves, without significant spalling or cracking; see Fig. 12(b). The enlarged area shows a microcrack formed in the wear track of model Cu-Ni-Mo-4SiC, see Fig. 12(a). The existence of pores at the contact surface may lead to localized stress concentration, which can reduce the strength of the Cu-Ni-Mo-4SiC composite. The EDS spectra of point C of the selected area are shown in Fig. 12(c). This adhesive wear area, which is composed of Cu-Ni-rich elements and SiC particles, aligns with their composition in wt% as demonstrated in Table 2. Point D shows the higher Mo (62.9 wt.%), Cu (22.4 wt.%), and O (5.4 wt.%) elements predominantly. Aside from the SiC particles, the presence of oxygen might contribute to tribo-oxide formation on the surface, which reduces the specific wear rate at the surface contact [39].

These observations confirm that the surface of the MA sample experienced mild abrasive wear,

which corresponds well with its high hardness and low specific wear rate. It is considered that the tribological performance improvement might be from a combination of both Mo and dispersion strengthening by SiC particles. The positive effect of the combination of refractory and SiC particles on increasing the wear resistance was obtained for Cu-Cr-W-SiC [40].

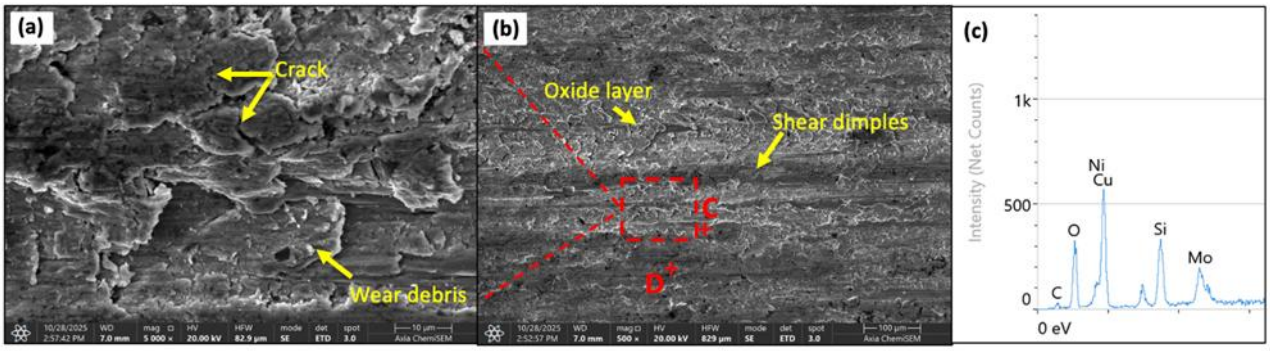

Fig. 12. (a) Enlarged area of the SEM image, (b) Morphologies of the wear surface of the Cu-Ni-Mo-4SiC composite for the MA mixing model, and (c) EDS spectra of selected areas (point C)

Table 3. Constituent elements of selected areas in Figs. 11 and 12

Mixing models	Points	Composition of the elements (wt.%)					
		Cu	Ni	Mo	Si	C	O
HM	A	49.6	41.9	0.1	0.4	5.2	2.8
	B	8.0	1.4	68.9	0.3	3.2	18.2
MA	C	89.9	4.6	1.3	0.6	1.7	1.9
	D	22.4	7.5	62.9	0.4	1.4	5.4

3.5. Electrical Properties

Fig. 13 illustrates the electrical characteristics of the Cu-Ni-Mo-4SiC composites fabricated using various mixing models. The highest electrical conductivity is 62% IACS, and the 2.78 × 10^{-8} Ωm resistivity is obtained for the MA technique. A higher electrical conductivity might be correlated with better microstructure and homogeneous particle distribution of this Cu-Ni-Mo-4SiC using MA mixing models, as shown in Fig. 6. On the other hand, the lowest conductivity is 55% IACS, while the highest resistivity exceeds 3.1 × 10^{-8} Ωm. Several factors, such as SiC dispersion, porosity formation, and contamination, are considered to contribute to the alloy's reduced conductivity. This condition is detrimental to the electrical conductivity of the Cu-Ni-Mo-4SiC synthesized by powder metallurgy through the HM mixing model. These results align with the mechanical properties and microstructure, in which the MA mixing model has a positive impact on the characteristics of the model Cu-Ni-Mo-4SiC composite.

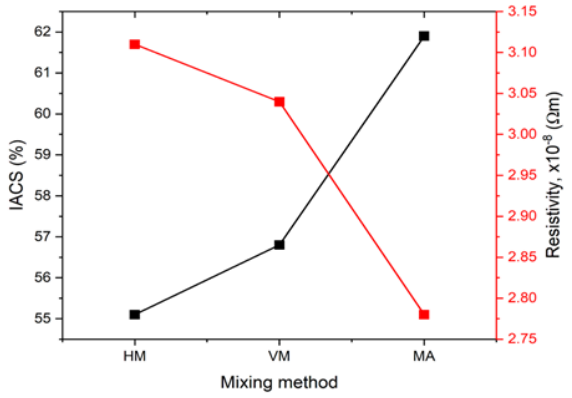

Fig. 13. Electrical properties of the Cu-Ni-Mo-4SiC composite under various mixing models

Mechanical alloying was most beneficial for the resulting microstructural homogeneity, hardness, wear resistance, and electrical conductivity in the Cu-Ni-5Mo-4SiC composite material, which is consistent with known effects of particle size reduction and even distribution due to high-energy milling [14, 18, 21]. Nevertheless, the above-mentioned findings are limited to a fixed composition with the Cu/Ni atomic ratio of 90/10 and 4 wt.%SiC, compaction pressure of 250 MPa; sintering at 770 °C for 1 h with a controlled heating rate of 16 °C/min until the temperature reaches 400 °C, after which the heating rate is reduced to

10 °C/min, respectively. Different compositions and process parameters change the microstructure, hardness, wear, and electrical properties. Furthermore, the limitation in the implementation to achieve the desired result is correlated with the presence of SiC particles, which might generate the agglomeration phenomenon and the difficulty of predicting agglomeration distribution.

4. CONCLUSION

In this study, HM, VM, and MA techniques were evaluated for Cu-Ni-Mo-4SiC composites. The major findings can be summarized as follows:

- The MA technique yielded the smallest crystallite size and the most uniform distribution of Mo and SiC phases in the Cu-Ni FCC matrix, thus proving the positive influence of increased mixing energy on the process.
- The highest hardness (65.1 HV), lowest specific wear rate (5.56×10^{-5} mm^3/Nm), lowest wear coefficient (3.55×10^{-5}) and electrical conductivity of 62% IACS were obtained by the MA composite.
- The enhanced performance of the MA composite was due to crystallite size reduction and uniformity in reinforcement distribution and particle detachment.
- VM had intermediate hardness, while it had the highest friction coefficient, which suggests that friction is affected by oxidation, wear particles, and tribo-film stability.
- Increased oxygen content in the worn surfaces demonstrated oxidative wear. The fracture of the oxide film caused delamination and abrasive wear.
- MA had the best mechanical, tribological, and electrical properties among the investigated specimens. The cost and energy efficiency of MA were not analyzed.
- The scientific contribution is the proven link between the mixing process, structure, reinforcing material distribution, and the functionality of the materials.
- The areas for further research include the study of protective sintering atmosphere, hot pressing, sintering conditions optimization, wear resistance, corrosion, fatigue, and MA energy consumption.

ACKNOWLEDGEMENTS

The authors sincerely acknowledge the financial support under the TALENTA research program from Universitas Sumatera Utara (USU) TA. 2025 with contract Number: 15497/UN5.1.R/PT.01.03/2025, July 17, 2025 (Batch II).

CONFLICTS OF INTEREST

The authors declare no competing interests.

REFERENCES

[1] M.R. Akbarpour, F. Gazani, H.M. Mirabad, I. Khezri, A. Moeini, N. Sohrabi, H.S. Kim, Recent advances in processing, and mechanical, thermal and electrical properties of Cu-SiC metal matrix composites prepared by powder metallurgy. *Progress in Materials Science*, 140, 2023: 101191. https://doi.org/10.1016/j.pmatsci.2023.101191

[2] J. Feng, K. Song, S. Liang, X. Guo, S. Li, Mechanical properties and electrical conductivity of oriented-SiC-whisker-reinforced Al_2O_3/Cu composites. *Journal of Materials Research and Technology*, 20, 2022: 1470-1480. https://doi.org/10.1016/j.jmrt.2022.07.131

[3] M. Gao, R. Bao, J. Yi, C. Li, J. Tao, Y. Ren, L. Du, Y. Zhao, C. Wu, L. Liu, Simultaneously enhanced strength and wear-resistance of Ti_3SiC_2 MAX phase reinforced Cu-Ni-Si composite via powder metallurgy method. *Journal of Alloys and Compounds*, 1023, 2025: 180168. https://doi.org/10.1016/j.jallcom.2025.180168

[4] Z. Moser, W. Zakulski, P. Spencer, K. Hack, Thermodynamic investigations of solid Cu Ni and Fe Ni alloys and calculation of the solid state miscibility gap in the Cu Fe Ni system, *Calphad*, 9(3), 1985: 257-269. https://doi.org/10.1016/0364-5916(85)90011-2

[5] T.D. Shen, C.C. Koch, Formation, solid-solution hardening and softening of nanocrystalline solid solutions prepared by mechanical attrition. *Acta Materialia*, 44(2), 1996: 753-761. https://doi.org/10.1016/1359-6454(95)00178-6

[6] C. Suryanarayana, Mechanical alloying and milling. *Progress in Materials Science*, 46(1–2), 2001: 1-184. https://doi.org/10.1016/S0079-6425(99)00010-9

[7] Z. Zhuang, Z. Li, L. Xu, Y. Feng, R. Wang, C. Peng, The influence of ball milling conditions on the powder characteristics and sintering densification of Mo-Cu alloy. *International Journal of Refractory Metals and Hard Materials*, 125, 2024: 106914. https://doi.org/10.1016/j.ijrmhm.2024.106914

[8] P. Cao, S. Liu, Y. Wu, Y. Xia, Z. Wu, Z. zhou, Y. Liu, A. Sun, Master sintering curve of binary mutually immiscible molybdenum-copper powders. *Journal of Alloys and Compounds*, 834, 2020: 155194. https://doi.org/10.1016/j.jallcom.2020.155194

[9] Y. Liang, Q. Lei, X. Zhang, D. Jiang, Y. Li, Microstructure evolution and properties of a Cu-5 wt.% Mo alloy with high conductivity and high anti-soften temperature. *Materials Today Communications*, 32, 2022: 104134. https://doi.org/10.1016/j.mtcomm.2022.104134

[10] M. Chen, N. Luo, Z. Wang, Q. Liu, B. Wang, B. Niu, J. Yang, X. Wu, Q. Li, J. He, Surface modification of highly reflective Cu powder using Mo particles as modifiers for improving energy efficiency in laser additive manufacturing of Cu-Mo immiscible alloys. *Journal of Manufacturing Processes*, 136, 2025: 251-266. https://doi.org/10.1016/j.jmapro.2025.01.069

[11] I. Cruz-Cruz, R. Hernández-Maya, J.E. Reséndiz-Hernández, O. Martínez-Romero, N.A. Ulloa Castillo, A. Elías-Zúñiga, Copper-Nickel/SiC composites for applications on contact electrodes. *Heliyon*, 10(22), 2024: e39965. https://doi.org/10.1016/j.heliyon.2024.e39965

[12] G.C. Efe, M. Ipek, S. Zeytin, C. Bindal, An investigation of the effect of SiC particle size on Cu-SiC composites. *Composites Part B: Engineering*, 43(4), 2012: 1813-1822. https://doi.org/10.1016/j.compositesb.2012.01.006

[13] M. Moakher, T. Shinbrot, F.J. Muzzio, Experimentally validated computations of flow, mixing and segregation of non-cohesive grains in three-dimensional tumbling blenders. *Powder Technology*, 109(1-3), 2000: 58-71. https://doi.org/10.1016/S0032-5910(99)00227-2

[14] A. Alexander, F.J. Muzzio, T. Shinbrot, Segregation patterns in V-blenders. *Chemical Engineering Science*, 58(2), 2003: 487-496. https://doi.org/10.1016/S0009-2509(02)00530-4

[15] C. Yin, Z. Wang, J. Yuan, Influence of powder mixing processes and WC contents on microstructure, shrinkage behavior, and mechanical properties of WC–Si_3N_4 composites. *Ceramics International*, 49(16), 2023: 26747-26758. https://doi.org/10.1016/j.ceramint.2023.05.211

[16] S. Mahmood, A. Iqbal, Rafi-ud-Din, A. Wadood, A. Mateen, M. Amin, I.S. Yahia, H.Y. Zahran, Influence of homogenizing methodology on mechanical and tribological performance of powder-metallurgy-processed titanium composites reinforced by graphene nanoplatelets. *Molecules*, 27(9), 2022: 2666. https://doi.org/10.3390/molecules27092666

[17] S.-J. Huang, Y.Y. Tanoto, C. Li, Effect of powder mixing on the mechanical strength of polyamide 6-AZ61 magnesium composites prepared by compression molding. *Composites Communications*, 53, 2025: 102169. https://doi.org/10.1016/j.coco.2024.102169

[18] A.M. Sankhla, K.M. Patel, M.A. Makhesana, K. Giasin, D.Y. Pimenov, S. Wojciechowski, N. Khanna, Effect of mixing method and particle size on hardness and compressive strength of aluminium-based metal matrix composite prepared through powder metallurgy route. *Journal of Materials Research and Technology*, 18, 2022: 282-292. https://doi.org/10.1016/j.jmrt.2022.02.094

[19] I. Dinaharan, T. Albert, Effect of reinforcement type on microstructural evolution and wear performance of copper matrix composites via powder metallurgy. *Materials Today Communications*, 34, 2023: 105250. https://doi.org/10.1016/j.mtcomm.2022.105250

[20] M.E. Cura, X.W. Liu, U. Kanerva, S. Varjus, A. Kivioja, O. Söderberg, S.P. Hannula, Friction behavior of alumina/molybdenum

composites and formation of MoO_{3-x} phase at 400 °C. *Tribology International*, 87, 2015: 23-31. https://doi.org/10.1016/j.triboint.2015.02.010

[21] Q. Zhang, J. Wang, B.-Y. Zhang, B.-H. Guo, J. Yu, Z.-X. Guo, Improved electrical conductivity of polymer/carbon-black composites by simultaneous dispersion and interaction-induced network assembly. *Composites Science and Technology*, 179, 2019: 106-114. https://doi.org/10.1016/j.compscitech.2019.05.008

[22] B. Krause, P. Pötschke, L. Häußler, Influence of small scale melt mixing conditions on electrical resistivity of carbon-nanotube-polyamide composites. *Composites Science and Technology*, 69(10), 2009: 1505-1515. https://doi.org/10.1016/j.compscitech.2008.07.007

[23] Z. Xiao, Y.-j. Ding, Z.-j. Wang, Y.-l. Jia, Y.-b. Jiang, S. Gong, Z. Li, Research and development of advanced copper matrix composites. *Transactions of Nonferrous Metals Society of China*, 34(12), 2024: 3789-3821. https://doi.org/10.1016/S1003-6326(24)66641-0

[24] A. Patra, R. Saxena, S.K. Karak, Combined effect of Ni and nano-Y_2O_3 addition on microstructure, mechanical and high temperature behavior of mechanically alloyed W-Mo. *International Journal of Refractory Metals and Hard Materials*, 60, 2016: 131-146. https://doi.org/10.1016/j.ijrmhm.2016.07.017

[25] C. Suryanarayana, Mechanical Alloying: A Novel Technique to Synthesize Advanced Materials. *Research*, 2019, 2019: 4219812. https://doi.org/10.34133/2019/4219812

[26] S. Gaona-Jimenez, R.A. Rodriguez-Diaz, A. Sedano, J. Porcayo-Calderon, A.M. Ocampo, S. Serna-Barquera, J.O. Olarte-Cortes, J.A. Juarez-Islas, Synthesis of a nanostructured Al–Cu powder alloy with additions of TiC particles by mechanical alloying and ball milling–mathematical modelling of microstructure. *Digest Journal of Nanomaterials and Biostructures*, 12(2), 2017: 449-462.

[27] B. Zhang, R. Zhao, B. Ren, A. Jiang, C. Chen, J. Liu, Y. Zhou, Mechanical Alloying Behavior and Thermal Stability of CoCrCuFeMnNix High-Entropy Alloy Powders Prepared via MA. *Materials*, 16(8), 2023: 3179. https://doi.org/10.3390/ma16083179

[28] C. Shuai, C. He, S. Peng, F. Qi, G. Wang, A. Min, W. Yang, W. Wang, Mechanical alloying of immiscible metallic systems: process, microstructure and mechanism. *Advanced Engineering Materials*, 23, 2021: 2001098. https://doi.org/10.1002/adem.202001098

[29] Y. Yu, W. Xiao, J. Wang, L. Wang, First-principles study of Mo segregation in MoNi(111): Effects of chemisorbed atomic oxygen. *Materials*, 9(1), 2016: 5. https://doi.org/10.3390/ma9010005

[30] C. Shu, K. Chen, H. Yang, M. Chen, X. He, Effect of V and ball milling time on microstructure and thermal properties of $CoCrCuFeNiV_x$ by mechanical alloying. *Physica B: Condensed Matter*, 571, 2019: 235-242. https://doi.org/10.1016/j.physb.2019.07.028

[31] H. Toda, T. Inamori, K. Horikawa, K. Uesugi, A. Takeuchi, Y. Suzuki, M. Kobayashi, Effects of hydrogen micropores on mechanical properties in A2024 aluminum alloys. *Materials Transactions*, 54(12), 2013: 2195-2201. https://doi.org/10.2320/matertrans.L-M2013832

[32] H.-W. Hwang, J.-H. Park, D.-G. Lee, Effect of molybdenum content on microstructure and mechanical properties of Ti–Mo–Fe alloys by powder metallurgy. *Applied Sciences*, 12(14), 2022: 7257. https://doi.org/10.3390/app12147257

[33] S. Hao, J. Li, K. Yamanaka, A. Chiba, Molybdenum segregation at grain boundaries in a nanograined Ni–Mo alloy: implications for yielding behavior and plastic deformation modes. *Computational Materials Science*, 256, 2025: 113973. https://doi.org/10.1016/j.commatsci.2025.113973

[34] W. Abd-Elaziem, A. Hamada, T. Allam, M.M. Mohammed, M. Abd-El Hamid, S. Samah, D. Wasfy, M. A. Darwish, Y.O.A.E. El-Kady, S. Elkatatny, Enhancement of mechanical and physical properties of Cu–Ni composites by various contents of Y_2O_3 reinforcement. *Journal of Materials Research and Technology*, 30, 2024: 473-484. https://doi.org/10.1016/j.jmrt.2024.03.075

[35] N.T. Câmara, R.A. Raimundo, C.S. Lourenco, L.M.F. Morais, D.D.S. Silva, R.M. Gomes, M.A.

Morales, D.A. Macedo, U.U. Gomes, F.A. Costa, Impact of the SiC addition on the morphological, structural and mechanical properties of Cu–SiC composite powders prepared by high energy milling. *Advanced Powder Technology*, 32(8), 2021: 2950-2961. https://doi.org/10.1016/j.apt.2021.06.006

[36] M.M.J. Sridhar, M. Ravichandran, G. Veerappan, Microstructure and properties of silicon carbide and yttrium oxide reinforced copper matrix hybrid composites (Cu–SiC–Y_2O_3). *Materials Research*, 28, 2024: 1-11. https://doi.org/10.1590/1980-5373-mr-2024-0406

[37] M.I. Abd El Aal, Wear properties of copper and copper composites powders consolidated by high-pressure torsion. *Friction*, 8(2), 2020: 433-450. https://doi.org/10.1007/s40544-019-0285-3

[38] E. Şap, Investigation of mechanical properties of Cu/Mo–SiCp composites produced with powder metallurgy and their wear behaviour using the Taguchi method. *Ceramics International*, 47(18), 2021: 25910-25920. https://doi.org/10.1016/j.ceramint.2021.05.322

[39] N. Vashishtha, S.G. Sapate, J.S. Gahlot, P. Bagde, Effect of tribo-oxidation on friction and wear behaviour of HVOF sprayed WC–10Co–4Cr coating. *Tribology Letters*, 66(56), 2018: 1-19. https://doi.org/10.1007/s11249-018-1006-1

[40] Y. Jiang, L. Xiao, Z. Peng, M. Li, J. Li, X. Wang, G. Deng, J. Fang, Z. Cai, X. Zhao, S. Liu, Laser cladding of heterogeneous structured Cu–Cr–W–SiC coatings with balanced electrical conductivity and wear resistance. *Materials & Design*, 254, 2025: 114009. https://doi.org/10.1016/j.matdes.2025.114009

© 2026 by the authors. This work is licensed under a Creative Commons Attribution-Non Commercial 4.0 International License (CC BY-NC 4.0).